Coordination Chemistry Reviews 254 (2010) 1871–1881

Contents lists available at ScienceDirect

Coordination Chemistry Reviews

journal homepage: www.elsevier.com/locate/ccr

Review

Structures and spin states of mono- and dinuclear iron(II) complexes of imidazole-4-carbaldehyde azine and its derivatives

Yukinari Sunatsuki [a], Ryohei Kawamoto [a], Kunihiro Fujita [a], Hisashi Maruyama [a], Takayoshi Suzuki [a], Hiroyuki Ishida [a], Masaaki Kojima [a,*], Seiichiro Iijima [b], Naohide Matsumoto [c]

[a] Department of Chemistry, Faculty of Science, Okayama University, Tsushima-naka 3-1-1, Okayama 700-8530, Japan
[b] National Institute of Advanced Industrial Science and Technology, Tsukuba 305-8566, Japan
[c] Department of Chemistry, Faculty of Science, Kumamoto University, Kurokami 2-39-1, Kumamoto 860-8555, Japan

Contents

ARTICLE INFO

Article history:
Received 31 July 2009
Accepted 16 November 2009
Available online 24 November 2009

Keywords:
Iron(II) complexes
Dinuclear complexes
Helicates
Spin-crossover
Spin states

ABSTRACT

Mononuclear $[Fe(H_2L^R)_2]X_2$ (R = H, 2-Me, 5-Me, 2-Et-5-Me; X = ClO_4, BF_4) and dinuclear $[Fe_2(H_2L^R)_3]X_4$ complexes containing imidazole-4-carbaldehyde azine (H_2L^H) and its derivatives prepared by condensation of 4-formylimidazole, 2-methyl- or 5-methyl-4-formylimidazole, or 2-ethyl-4-methyl-5-formylimidazole, with hydrazine in a 2:1 mole ratio in methanol, were prepared and their magnetostructural relationships were studied. In the mononuclear complexes, H_2L^R acts as an unsymmetrical tridentate ligand with two imidazole nitrogen atoms and one azine nitrogen atom, while in the dinuclear complexes, H_2L^R acts as a dinucleating ligand employing four nitrogen atoms to form a triple helicate structure. At room temperature, $[Fe_2(H_2L^H)_3](ClO_4)_4$ and $[Fe_2(H_2L^{2\text{-Me}})_3](ClO_4)_4$ were in the high-spin (HS) and low-spin (LS) states, respectively. The results are in accordance with the ligand field strength of $H_2L^{2\text{-Me}}$ with electron-donating methyl groups being stronger than H_2L^H, with the order of the ligand field strengths being $H_2L^{2\text{-Me}} > H_2L^H$. However, in the mononuclear $[Fe(H_2L^H)_2](ClO_4)_2$ and $[Fe(H_2L^{2\text{-Me}})_2](ClO_4)_2$ complexes, a different order of ligand field strengths, $H_2L^H > H_2L^{2\text{-Me}}$, was observed because $[Fe(H_2L^H)_2](ClO_4)_2$ was in the LS state while $[Fe(H_2L^{2\text{-Me}})_2](ClO_4)_2$ was in the HS state at room temperature. X-ray structural studies revealed that the interligand steric repulsion between a methyl group of an $H_2L^{2\text{-Me}}$ ligand and the other ligand in $[Fe(H_2L^{2\text{-Me}})_2](ClO_4)_2$ is responsible for the observed change in the spin state. The same is true for $[Fe(H_2L^{2\text{-Et-5-Me}})_2](ClO_4)_2$, while $[Fe(H_2L^{5\text{-Me}})_2](ClO_4)_2$ does not involve such a steric congestion and stays in the LS state over the temperature range 5–300 K. Two kinds of crystals (polymorphs) were isolated for $[Fe_2(H_2L^H)_3](BF_4)_4$ and $[Fe_2(H_2L^{2\text{-Et-5-Me}})_3](ClO_4)_4$, and they exhibited different magnetic behaviors.

1. Introduction

Increasing attention is being paid to bistable molecules because they can be used as molecular memories and switches in electronic devices [1]. The phenomenon of spin-crossover (SCO) between the

* Corresponding author. Tel.: +81 86 251 7842; fax: +81 86 251 7842.
E-mail address: kojima@cc.okayama-u.ac.jp (M. Kojima).

0010-8545/$ – see front matter © 2009 Elsevier B.V. All rights reserved.
doi:10.1016/j.ccr.2009.11.016

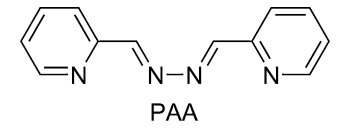

PAA

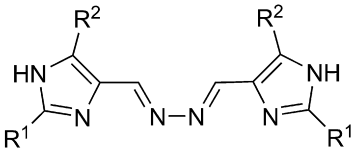

H_2L^{H}: $R^1 = R^2 = H$
$H_2L^{2\text{-Me}}$: $R^1 = Me$, $R^2 = H$
$H_2L^{5\text{-Me}}$: $R^1 = H$, $R^2 = Me$
$H_2L^{2\text{-Et-5-Me}}$: $R^1 = Et$, $R^2 = Me$

Scheme 1. Ligands, PAA, H_2L^{H}, $H_2L^{2\text{-Me}}$, $H_2L^{5\text{-Me}}$ and $H_2L^{2\text{-Et-5-Me}}$.

low-spin (LS) and high-spin (HS) states is the most spectacular example of molecular bistability. SCO is observed in some octahedral $3d^n$ ($4 \le n \le 7$) metal complexes, the first report being for the Fe^{III} complex of dithiocarbamates, as a result of variation in temperature, by Cambi and Szegö [2]. Early in the 1960s, Busch and co-workers were attempting to identify the crossover region for Fe^{II} and Co^{II} [3], and reported the first instance of SCO in a complex of the latter ion [4]. The spin state can be fine-tuned by external perturbations such as variation in the temperature or pressure, or light or X-ray irradiation, or even exchange of counterions or solvent molecules [5]. It has recently been demonstrated that the spin transition may also be stimulated by solid–liquid crystal, order–disorder phase transitions, and guest absorption–desorption [5].

The coordination chemistry of 2-pyridinealdazine (=pyridine-2-carbaldehyde azine, PAA; Scheme 1) was first described by Stratton and Busch in papers in 1958 and 1960 [6]; their studies are of particular historical importance to the field of metallosupramolecular chemistry, and in particular to helicate formation. These workers described the coordination of PAA to octahedral transition metal ions to form complexes with the formula $[M_2(PAA)_3]^{4+}$ (M = Co, Fe, and Ni), where PAA acts as a dinucleating ligand employing all four nitrogen atoms. The helical complexes were shown to undergo exchange reactions on heating or standing in methanol to form mononuclear complexes $[M(PAA)_2]^{2+}$ in which PAA acts as an unsymmetrical tridentate ligand with two pyridyl nitrogen atoms and one azine nitrogen atom (Scheme 2). They proposed the term "flexidentate" to describe the coordination behavior of the ligand [6]. In 2002, Hannon and co-workers obtained crystals of the hexafluorophosphate salt of Stratton and Busch's original iron(II) complex, $[Fe_2(PAA)_3](PF_6)_4{\cdot}4CH_3NO_2$, and confirmed the triple helicate structure by X-ray diffraction [7].

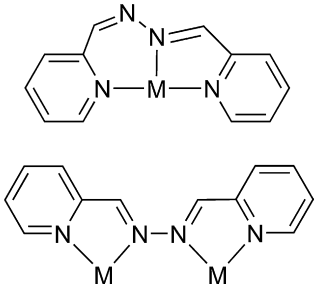

Scheme 2. Two coordination modes adopted by PAA.

Both of the iron(II) complexes, $[Fe(PAA)_2]^{2+}$ and $[Fe_2(PAA)_3]^{4+}$, were reported to be in the LS state [6]. An imidazole nitrogen atom usually exhibits a weaker ligand field strength than does a pyridine nitrogen atom [8], and we expect that the imidazole analogue of PAA, H_2L^{H}, and its derivatives, $H_2L^{2\text{-Me}}$, $H_2L^{5\text{-Me}}$, and $H_2L^{2\text{-Et-5-Me}}$ (Scheme 1), will have the necessary ligand field strength to form SCO iron(II) complexes. The incorporation of imidazole groups has another advantage because the uncoordinated NH groups can be involved in hydrogen-bond formation to increase cooperativity. For example, we have reported that Fe complexes with a tripodal ligand involving three imidazole groups have a two-dimensional (2D) extended network structure based on imidazole–imidazolate hydrogen bonds and that they exhibit steep and multistep SCO behaviors [8].

Dinuclear SCO Fe^{II} complexes have attracted attention because they can combine two properties such as magnetic coupling and SCO in the same molecule, as well as having the possibility of investigating new cooperative behavior [9]. In such complexes, the iron centers are coupled by intramolecular interactions, and three different spin-pair states, [LS–LS], [LS–HS], and [HS–HS], are possible. Actually, some complexes exhibit a two-step SCO phenomenon, [LS–LS] ↔ '[LS–HS]' ↔ [HS–HS] [10,11]. However, the half-SCO species, '[LS–HS]', can consist of either a 1:1 mixture of [LS–LS] and [HS–HS] complexes or a distinct [LS–HS] complex. Kaizaki and co-workers reported that the '[LS–HS]' species of their doubly pyrazolate-bridged two-step SCO diiron(II) complex is a mixture of [LS–LS] and [HS–HS] complexes [11]. Recently, Brooker and co-workers confirmed for the first time the existence of the mixed-spin state [LS–HS] from X-ray crystallographic data of the doubly 1,2,4-triazole-bridged complex [12]. Amoore et al. structurally characterized the three spin states, [LS–LS], [LS–HS], and [HS–HS], for the first time [10 g]. Only a limited number of papers have dealt with dinuclear Fe^{II} SCO helicate complexes. Williams et al. have reported an Fe^{II} helicate involving benzimidazole ligands showing two-step SCO [13]. The Fe^{II}–imidazolimine complexes with a supramolecular triple-helicate structure exhibiting various SCO behaviors were also studied [7,14]. The SCO of this system was reinterpreted by Gütlich and co-workers [15]. Very recently, Pelleteret et al. reported LIESST (light-induced excited spin state trapping) in a dinuclear Fe^{II} helicate with ligands containing imidazolimine groups [16].

We have reported the synthesis, characterization, structure, and magnetic properties of mononuclear $[Fe(H_2L^{R})_2]^{2+}$ (R = H, 2-Me, 5-Me, 2-Et-5-Me) and dinuclear $[Fe_2(H_2L^{R})_3]^{4+}$ complexes, where H_2L^{H}, $H_2L^{2\text{-Me}}$, $H_2L^{5\text{-Me}}$, and $H_2L^{2\text{-Et-5-Me}}$ denote imidazole-4-carbaldehyde azine, 2-methylimidazole-4-carbaldehyde azine, 5-methylimidazole-4-carbaldehyde azine, and 2-ethyl-5-methylimidazole-4-carbaldehyde azine, respectively [17,18]. Comparison of the SCO behaviors of the mononuclear complexes with those of the dinuclear triple-helicate complexes involving the same ligands is particularly important in studying the structural effects.

2. Synthesis and characterization

The synthetic procedures yielding the H_2L^{R} (R = H, 2-Me, 5-Me, 2-Et-5-Me) ligands and the Fe^{II} complexes are shown schematically in Fig. 1. The ligands were prepared by condensation of 4-formylimidazole, or its derivatives, 2-methyl- or 5-methyl-4-formylimidazole, or 2-ethyl-4-methyl-5-formylimidazole, with hydrazine in a 2:1 mole ratio in methanol.

The mononuclear complex, $[Fe(H_2L^{H})_2](ClO_4)_2{\cdot}CH_3OH$ (**1H·ClO$_4$**), was prepared by reaction of H_2L^{H} and $Fe(ClO_4)_2{\cdot}6H_2O$ in a 2:1 mole ratio in methanol. The color of the mixture changed from orange to dark purple as the reaction proceeded; on addition of diethyl ether, the perchlorate of **1H**, $[Fe(H_2L^{H})_2](ClO_4)_2{\cdot}CH_3OH$

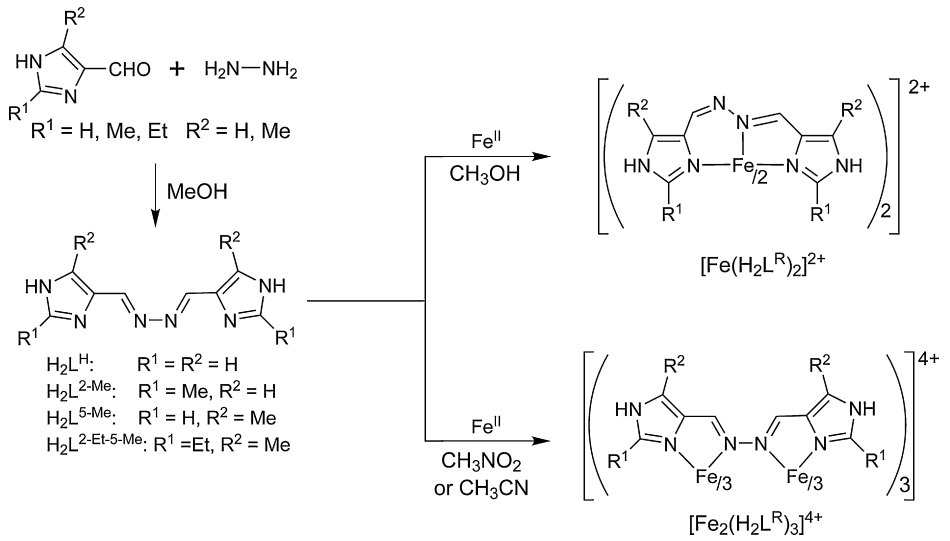

Fig. 1. Synthetic procedures yielding the H_2L^R (R = H, 2-Me, 5-Me, 2-Et-5-Me) ligands and the mononuclear and dinuclear Fe^{II} complexes.

(**1H·ClO$_4$**), was isolated as dark purple crystals. A similar color change from red to blue was reported during the preparation of $[Fe(PAA)_2]^{2+}$. The helical $[Fe_2(PAA)_3]^{4+}$ complex, which formed first, underwent exchange reactions on heating or standing in methanol to form the mononuclear complex $[Fe(PAA)_2]^{2+}$ [6]. Thus, **1H** is suggested to form by way of the dinuclear complex, $[Fe_2(H_2L^H)_3]^{4+}$ (**2H**). The corresponding 2-methyl, 5-methyl, and 2-ethyl-5-methyl derivatives, $[Fe(H_2L^{2\text{-}Me})_2](ClO_4)_2\cdot H_2O$ (**1Me·ClO$_4$**), $[Fe(H_2L^{5\text{-}Me})_2](ClO_4)_2\cdot 1.5H_2O$ (**1Me′·ClO$_4$**), and $[Fe(H_2L^{2\text{-}Et\text{-}5\text{-}Me})_2](ClO_4)_2\cdot CH_3OH$ (**1EtMe·ClO$_4$**), were prepared in a similar manner and isolated as reddish orange or dark purple crystals. The distinct color difference, dark purple (**1H·ClO$_4$**, **1Me′·ClO$_4$**) versus reddish orange (**1Me·ClO$_4$**, **1EtMe·ClO$_4$**), suggested that the complexes were in different spin states (Fig. 2).

The dinuclear complexes, $[Fe_2(H_2L^H)_3](ClO_4)_4$ (**2H·ClO$_4$**), $[Fe_2(H_2L^{2\text{-}Me})_3](ClO_4)_4$ (**2Me·ClO$_4$**), and $[Fe_2(H_2L^{5\text{-}Me})_3](ClO_4)_4$ (**2Me′·ClO$_4$**), were prepared by reaction of the respective ligand and $Fe(ClO_4)_2\cdot 6H_2O$ in nitromethane or acetonitrile in a 3:2 mole ratio. The analogous yellow 2-Et-5-Me derivative was a mixture of plate crystals, $[Fe_2(H_2L^{2\text{-}Et\text{-}5\text{-}Me})_3](ClO_4)_4\cdot 0.5H_2O\cdot 3CH_3CN$ (**2EtMe·ClO$_4$-plate**), and block crystals, $[Fe_2(H_2L^{2\text{-}Et\text{-}5\text{-}Me})_3](ClO_4)_4\cdot 2CH_3CN$ (**2EtMe·ClO$_4$-block**). They were separated manually under a microscope.

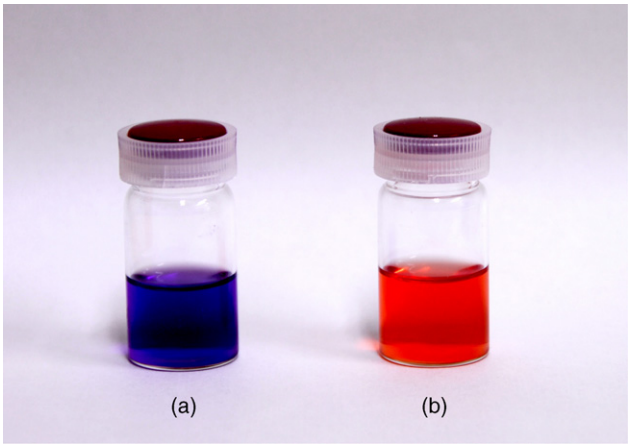

Fig. 2. (a) $[Fe(H_2L^H)_2](ClO_4)_2$ (**1H·ClO$_4$**) in methanol, and (b) $[Fe(H_2L^{2\text{-}Me})_2](ClO_4)_2$ (**1Me·ClO$_4$**) in methanol.

The dinuclear complexes are stable only in such solvents as nitromethane and acetonitrile. The instability of the complexes in such solvents as methanol and *N,N*-dimethylformamide may be related to the higher coordinating ability of these solvent molecules. Because of this instability, it was difficult to exchange the counter ions of the dinuclear complexes. The tetrafluoroborates of the dinuclear complexes were prepared by reaction of $Fe(BF_4)_2\cdot 6H_2O$ and H_2L^R in nitromethane or acetonitrile. As in the case of **2EtMe·ClO$_4$**, the $[Fe_2(H_2L^H)_3](BF_4)_4\cdot 7CH_3NO_2$ (**2H·BF$_4$**) complex was isolated in two types of crystal forms, needles (**2H·BF$_4$-needle**) and blocks (**2H·BF$_4$-block**), on crystallization from nitromethane by slow diffusion of diethyl ether. The crystals were separated manually under a microscope. Crystal solvents of the samples of **2H·BF$_4$** were easily lost on drying in vacuo, and such samples were used for magnetic studies.

The IR spectra of the H_2L^R (R = H, 2-Me, 5-Me, 2-Et-5-Me) ligands showed strong characteristic absorptions at 1625–1639 cm^{-1}, assignable to the C=N stretching vibration [19]. The dinuclear complexes showed one ν(C=N) band in the 1617–1634 cm^{-1} region, while the mononuclear complexes showed two bands in the 1559–1594 and 1622–1630 cm^{-1} regions. The number of ν(C=N) bands, one for the dinuclear complexes and two for the mononuclear complexes, is in accordance with the symmetry of the complexes, because in the mononuclear complexes, the H_2L^R ligand functions as an unsymmetrical tridentate ligand. The ν(C=N) bands of the dinuclear complexes were not as sharp as those of the ligands and the mononuclear complexes, and this may be related to the fact that the two Fe^{II} sites are not equivalent (see below). The electron density in the C=N moiety is donated to a metal upon coordination, and the double-bond character decreases and the position of the ν(C=N) band should shift to the lower wavenumber region. Thus, the bands in the lower wavenumber region of the mononuclear complexes (1559–1594 cm^{-1}) can be assigned to the coordinated C=N moiety. The bands in the higher wavenumber region (1622–1630 cm^{-1}) are observed near those of the free ligands (1625–1639 cm^{-1}), and they can be safely assigned to the uncoordinated C=N moiety.

UV–vis spectral data of the mononuclear (**1H**, **1Me**, **1Me′**, **1EtMe**) and dinuclear (**2H**, **2Me**, **2Me′**, **2EtMe**) complexes in acetonitrile at 295 K are listed in Table 1. All complexes have an intense absorption band attributable to the metal-to-ligand charge-transfer transition in the visible region, which is responsible for the deep color, and thus weak d–d bands are obscured. The **1H** and **1Me′**

Table 1
UV–vis spectral data of the H_2L^H ligand in methanol, and the mononuclear (**1H**, **1Me**, **1Me′**, **1EtMe**) and the dinuclear (**2H**, **2Me**, **2Me′**, **2EtMe**) complexes in acetonitrile at 295 K.

Compound	λ_{max}/nm (ε/M^{-1} cm^{-1})
H_2L^H	205 (9300) 312 (33,600)
1H	301(29,700) 326 (25,800) 343 (21,900) 363 (sh, 6360) 557 (3840)
1Me	330 (64,100) 488 (820)
1Me′	348 (35,900) 410 (sh, 1380) 556 (4070)
1EtMe	350 (51,600) 446 (987)
2H	293 (56,300) 463 (4790) 570 (sh, 830)
2Me	306 (61,700) 467 (sh, 1100) 565 (sh, 180)
2Me′	319 (55,200) 463 (sh, 4210) 570 (sh,1230)
2EtMe	315 (59,800) 460 (sh, 1100) 600 (sh, 70)

complexes are in the LS state and show a strong absorption in the longer wavelength region (Fig. 3). The **1Me** and **1EtMe** complexes that are in the HS state show a strong band in the shorter wavelength region (**1Me**: 488 nm; **1EtMe**: 446 nm) [20]. All complexes have an intense band at 293–350 nm assignable to the imine π–π^* transition of the ligands.

The electrochemical properties of **1H** and **1Me** were studied by cyclic voltammetry (CV). The measurements were performed under nitrogen with a glassy carbon working electrode using an acetonitrile solution containing $(n\text{-}Bu)_4NBF_4$ (0.1 M) as supporting electrolyte. The redox couple ($Fe^{III/II}$) of **1H** appears at +0.291 V (E_{pc} = +0.256 V, E_{pa} = +0.325 V) versus Ag/Ag^+ irrespective of the scan rate ($10 \le \nu \le 200$ mV s^{-1}), the peak current ratio i_{pa}/i_{pc} was found to be 1.0, (i_{pa} or i_{pc})/$\nu^{1/2}$ was independent of ν, and the peak separation was 69 mV (Fig. 4). These results are consistent with an electrochemically reversible one-electron process; see Eq. (1)

$$[Fe^{III}(H_2L^H)_2]^{3+} + e^- \rightleftarrows [Fe^{II}(H_2L^H)_2]^{2+} \quad (1)$$

The methyl derivative, **1Me**, shows the reversible $Fe^{III/II}$ redox couple at $E^{o\prime}$ = +0.444 V (E_{pc} = +0.410 V, E_{pa} = +0.478 V, ΔE_{pa} = 68 mV) versus Ag/Ag^+, which is more positive than that for **1H** by 0.153 V. In general, as the electron-donating ability of the substituent increases, the observed potential shifts in the cathodic (less positive) direction and the higher oxidation state of the metal is stabilized [21]. This implies that the substituent group directly affects the electron density present on the metal atom. The greater the electron density present on the metal atom as a result of the electronic properties of the substituent group, the more difficult it should be to perform a reduction. Thus, replacement of hydrogen atoms with electron-donating methyl groups would make the compound easier to oxidize (i.e., the redox potential becomes less positive). The unexpected result that **1Me** is more difficult to oxidize than **1H** seems to be related to the different spin states of the complexes. The effect of the spin state on the redox potential has been pointed out for other Fe^{II} complexes [22].

CVs for the dinuclear complexes, **2H** and **2Me**, were measured under the same conditions as for the mononuclear complexes. The $Fe^{III/II}$ redox couple was irreversible for both complexes. The anodic peak was observed at E_{pa} = +0.705 V for **2H** and at E_{pa} = +0.690 V for **2Me**, while the cathodic peak was not observed clearly for either complex. The less positive E_{pa} value for **2Me** is consistent with the presence of electron-donating methyl groups and its LS state. The irreversible nature may be related to instability of the dinuclear complexes in the Fe^{III} state.

3. Spin states of the complexes

3.1. Spin states of the mononuclear complexes

The magnetic behaviors of $[Fe(H_2L^H)_2](ClO_4)_2$ (**1H·ClO$_4$**), $[Fe(H_2L^{2\text{-}Me})_2](ClO_4)_2$ (**1Me·ClO$_4$**), and $[Fe(H_2L^{2\text{-}Et\text{-}5\text{-}Me})_2](ClO_4)_2$ (**1EtMe·ClO$_4$**) are shown in Fig. 5 in the form of $\chi_M T$ versus T plots, where χ_M is the molar magnetic susceptibility and T is the absolute temperature. The mononuclear **1H·ClO$_4$** complex remains in the LS state over the range 5–300 K. The $\chi_M T$ values of 3.40 cm^3 K mol^{-1} of **1Me·ClO$_4$** and 3.65 cm^3 K mol^{-1} of **1EtMe·ClO$_4$** at 300 K are within the range of expected values for a paramagnetic Fe^{II} in its HS state with some orbital contributions. The drop of $\chi_M T$ below 50 K is probably due to zero-field splitting (ZFS) of Fe^{II} in the HS state. The magnetic measurements clearly indicate that **1H·ClO$_4$** is in the LS state, while **1Me·ClO$_4$** and **1EtMe·ClO$_4$** are in the HS states, at least above 50 K. These results are unexpected, because the ligand field strength of the $H_2L^{2\text{-}Me}$ and $H_2L^{2\text{-}Et\text{-}5\text{-}Me}$ ligands will be larger than that of the H_2L^H ligand because of the presence of electron-donating alkyl groups, and **1Me·ClO$_4$** and **1EtMe·ClO$_4$** are expected to be in the LS state. The existence of **1Me·ClO$_4$** (or **1EtMe·ClO$_4$**) in the HS state can be explained in terms of intramolecular steric repulsion between a methyl group of an $H_2L^{2\text{-}Me}$ ligand (or an ethyl group of an $H_2L^{2\text{-}Et\text{-}5\text{-}Me}$ ligand) and the other ligand in the complex (see below). The $[Fe(H_2L^{5\text{-}Me})_2](ClO_4)_2$ (**1Me′·ClO$_4$**) complex does not involve such a steric congestion, and the $\chi_M T$ value stays at almost

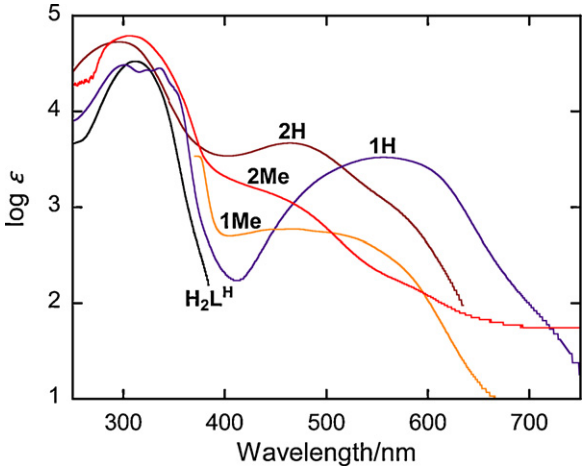

Fig. 3. UV–vis spectra for the H_2L^H ligand (black) in methanol, and mononuclear $[Fe(H_2L^H)_2]^{2+}$ (**1H**, purple), dinuclear $[Fe_2(H_2L^H)_3]^{4+}$ (**2H**, brown), mononuclear $[Fe(H_2L^{2\text{-}Me})_2]^{2+}$ (**1Me**, orange) and dinuclear $[Fe_2(H_2L^{2\text{-}Me})_3]^{4+}$ (**2Me**, red), in acetonitrile at 295 K. Reproduced with permission from Ref. [17b].

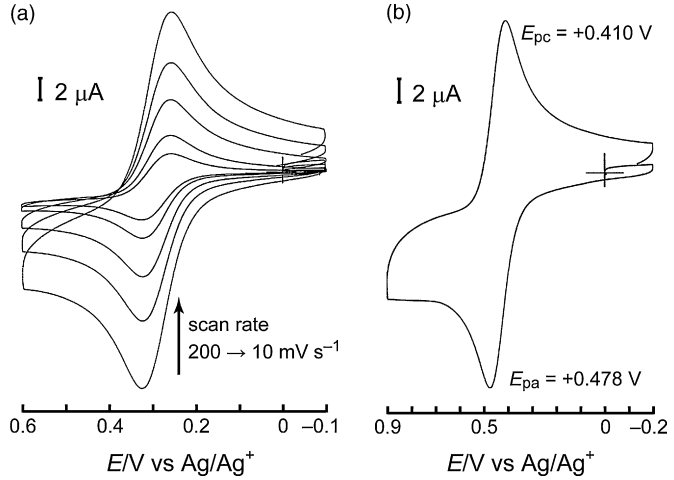

Fig. 4. (a) Cyclic voltammograms of $[Fe(H_2L^H)_2]^{2+}$ (**1H**) in acetonitrile containing 0.1 M $(n\text{-}Bu)_4NBF_4$ at a glassy carbon electrode as a function of the sweep rate: 10, 20, 50, 100, and 200 mV s^{-1}. (b) CV of $[Fe(H_2L^{2\text{-}Me})_2]^{2+}$ (**1Me**) under the same conditions as for (a) at 100 mV s^{-1}. Reproduced with permission from Ref. [17b].

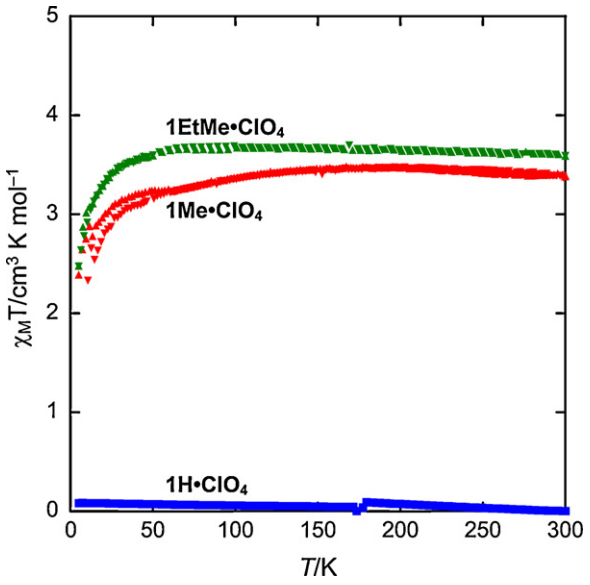

Fig. 5. Magnetic behaviors of $[Fe(H_2L^{H})_2](ClO_4)_2$ (**1H·ClO$_4$**); blue, $[Fe(H_2L^{2\text{-}Me})_2](ClO_4)_2$ (**1Me·ClO$_4$**); red, and $[Fe(H_2L^{2\text{-}Et\text{-}5\text{-}Me})_2](ClO_4)_2$ (**1EtMe·ClO$_4$**); green in the form of $\chi_M T$ versus T plots. The samples were quickly cooled from 300 to 5 K, and χ_M was measured successively during heating (5–300 K, ▲) and cooling (300–5 K, ▼) modes, at a sweep rate of 2 K min^{-1}.

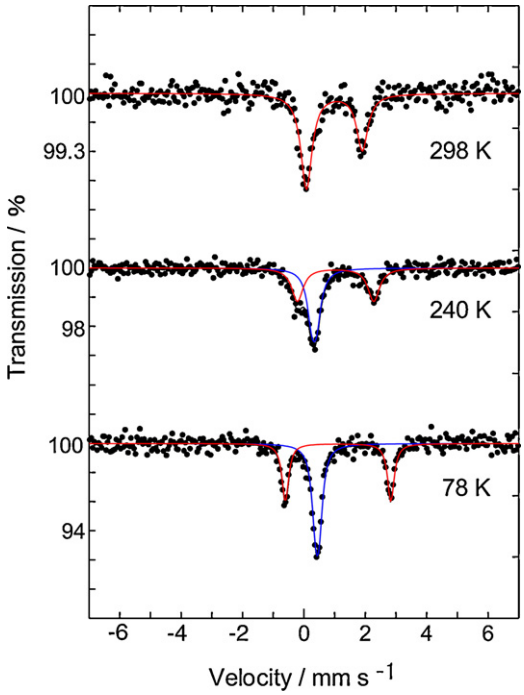

Fig. 7. Mössbauer spectra for $[Fe_2(H_2L^{H})_3](ClO_4)_4$ (**2H·ClO$_4$**) at 78, 240, and 298 K. Reproduced with permission from Ref. [17b].

0 cm^3 K mol^{-1} over the whole temperature range, demonstrating the LS state. The substituent effect on the spin equilibrium was also observed for Fe^{II} complexes with hexadentate ligands [22].

3.2. Spin states of the dinuclear complexes

The magnetic behaviors of $[Fe_2(H_2L^{H})_3](ClO_4)_4$ (**2H·ClO$_4$**), $[Fe_2(H_2L^{2\text{-}Me})_3](ClO_4)_4$ (**2Me·ClO$_4$**), and $[Fe_2(H_2L^{2\text{-}Et\text{-}5Me})_3](ClO_4)_4$ (**2EtMe·ClO$_4$**) are shown in Fig. 6 in the form of a $\chi_M T$ versus T plot. Complex **2Me·ClO$_4$** remained in the LS state over the entire temperature range, and this result is in accordance with the strong ligand field strength of the $H_2L^{2\text{-}Me}$ ligand caused by the presence of electron-donating methyl groups.

Complex **2H·ClO$_4$** exhibited an abrupt SCO behavior at ca. 240 K. Above 250 K, the $\chi_M T$ value was nearly constant at 6.6 cm^3 K mol^{-1}, which is close to the calculated spin-only value for the magnetically uncoupled [HS–HS] system ($\chi_M T$ = 6.0 cm^3 K mol^{-1}). In the temperature range 30–220 K, the value of $\chi_M T$ was nearly constant at 3.3 cm^3 K mol^{-1}, indicating that 50% of the Fe^{II} sites were in the HS state. The half-SCO state was trapped, the complex was locked into it, and it did not change into the [LS–LS] state on further cooling. The decrease in $\chi_M T$ observed below about 20 K is probably due to the ZFS effect [14]. That the half-SCO species of **2H·ClO$_4$** has a mixed-spin state, [LS–HS], was verified by X-ray crystal structure analysis (see below).

The temperature dependence of the Mössbauer spectra of **2H·ClO$_4$** agrees with the magnetic susceptibility results. At 298 K, the Mössbauer spectrum consists of a single quadrupole doublet (δ = 0.99 mm s^{-1}, ΔE_Q = 1.82 mm s^{-1}), demonstrating the sole existence of HS Fe^{II} (Fig. 7). We noticed that the bands were broad, with a full width at half-height of Γ = 0.44 mm s^{-1}, suggesting that

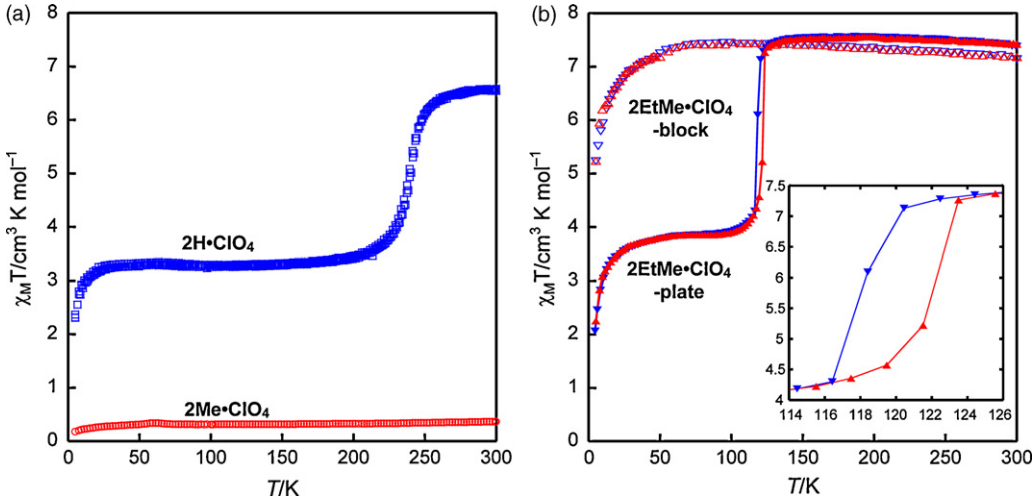

Fig. 6. (a) Magnetic behaviors of $[Fe_2(H_2L^{H})_3](ClO_4)_4$ (**2H·ClO$_4$**, blue) and $[Fe_2(H_2L^{2\text{-}Me})_3](ClO_4)_4$ (**2Me·ClO$_4$**, red) in the form of a $\chi_M T$ versus T plot. (b) Magnetic behavior of $[Fe_2(H_2L^{2\text{-}Et\text{-}5\text{-}Me})_3](ClO_4)_4{\cdot}H_2O$ (**2EtMe·ClO$_4$-plate** ▲ and ▼) and $[Fe_2(H_2L^{2\text{-}Et\text{-}5\text{-}Me})_3](ClO_4)_4{\cdot}0.5CH_3CN$ (**2EtMe·ClO$_4$-block** △ and ▽) in the form of $\chi_M T$ versus T plots. The inset of b) shows a hysteresis observed for **2EtMe·ClO$_4$-plate**; $T_c\uparrow$ = 122 K and $T_c\downarrow$ = 118 K with ΔT = 4 K.

the Fe^{II} sites are not equivalent. This was confirmed by the X-ray crystal structure analysis (see below). At 78 K, the spectrum consists of two doublets exhibiting quadrupole splitting (HS Fe^{II}, $\delta = 1.11\ mm\ s^{-1}$, $\Delta E_Q = 3.44\ mm\ s^{-1}$, and $\Gamma = 0.26\ mm\ s^{-1}$; LS Fe^{II}, $\delta = 0.44\ mm\ s^{-1}$, $\Delta E_Q = 0.12\ mm\ s^{-1}$, and $\Gamma = 0.29\ mm\ s^{-1}$). Deconvolution of the spectrum at 78 K revealed the mole fraction of the HS Fe^{II} species to be 44%. These results agree with the magnetic susceptibility results.

We expected that the $H_2L^{2\text{-Et-5Me}}$ ligand would not be suited for constructing SCO complexes, because the ligand has two electron-donating groups on each imidazole ring and the magnitude of the ligand-field strength would be too large to cause SCO. In reality, the dinuclear $[Fe_2(H_2L^{2\text{-Et-5Me}})_3]^{4+}$ complexes have a ligand field strength around the SCO point. As described above, $[Fe_2(H_2L^{2\text{-Et-5Me}})_3](ClO_4)_4$ (**2EtMe·ClO$_4$**) was obtained in two crystal forms, plates and blocks, and they exhibited completely different magnetic behaviors (Fig. 6(b)). The block crystals, $[Fe_2(H_2L)_3](ClO_4)_4{\cdot}0.5CH_3CN$ (**2EtMe·ClO$_4$-block**), stayed in the HS state at least above 50 K, and the profile suggests that the antiferromagnetic interaction between the Fe sites would be quite small. The plate crystals, $[Fe_2(H_2L)_3](ClO_4)_4{\cdot}H_2O$ (**2EtMe·ClO$_4$-plate**), exhibited an abrupt spin transition at ca. 120 K accompanied by a hysteresis, $T_c\uparrow = 122$ K and $T_c\downarrow = 118$ K with $\Delta T_c = 4$ K. Above 125 K, the $\chi_M T$ value was nearly constant at $7.53\ cm^3\ K\ mol^{-1}$, which is larger than the calculated spin-only value for the [HS–HS] system ($\chi_M T = 6.0\ cm^3\ K\ mol^{-1}$) but in the range of the [HS–HS] systems reported so far [13]. In the temperature range 50–100 K, the value of $\chi_M T$ was nearly constant at $3.85\ cm^3\ K\ mol^{-1}$, indicating that 50% of the Fe^{II} sites were in the HS state. The decrease in $\chi_M T$ observed below ca. 50 K is probably due to the ZFS effect. The X-ray crystal structure analysis verified that the half-SCO species of **2EtMe·ClO$_4$-plate** assumes a mixed-spin state, [LS–HS] (see below). The correlation between the structure and magnetic properties of the two forms of **2EtMe·ClO$_4$** will be discussed later, in Section 4.

We also prepared the tetrafluoroborates of the dinuclear complexes to study the effect of the anions. As described above, $[Fe_2(H_2L^H)_3](BF_4)_4$ (**2H·BF$_4$**) was obtained in two kinds of crystals, needles (**2H·BF$_4$-needle**) and blocks (**2H·BF$_4$-block**), just as for **2EtMe·ClO$_4$**, and they exhibited different SCO behaviors. **2H·BF$_4$-needle** showed an abrupt spin transition at 254 K (Fig. 8) with behavior similar to that of **2H·ClO$_4$**. **2H·BF$_4$-block** exhibited a more abrupt spin transition at about 190 K accompanied by a hysteresis, $T_c\uparrow = 190$ K and $T_c\downarrow = 183$ K with $\Delta T = 7$ K (Fig. 8). The correlation between the structure and magnetic properties of the two forms of **2H·BF$_4$** will be discussed later, in Section 4. Differential scanning calorimetric measurements of the two crystal forms of **2H·BF$_4$** were carried out in the 120–280 K temperature range at a rate of $5\ K\ min^{-1}$. The temperature dependence of heat flow during heating and cooling for the two samples is shown in Fig. 9. Anomalies in the heat flow for the needle crystals appear during heating at $T_c\uparrow = 258.0$ K and $T_c\downarrow = 257.2$ K during cooling. These values agree reasonably well with those observed from the $\chi_M T$ versus T plot. The block crystals exhibited anomalies in the heat flow at $T_c\uparrow = 188.7$ K and $T_c\downarrow = 182.4$ K, which match reasonably well with the magnetic data. A shoulder observed in the heating mode may be due to the presence of an impurity.

4. X-ray crystal structures

4.1. Structures of the $H_2L^{2\text{-Me}}$ and $H_2L^{2\text{-Et-5-Me}}$ ligands

Crystals of $H_2L^{2\text{-Me}}$ and $H_2L^{2\text{-Et-5-Me}}$ suitable for X-ray crystal structure analysis were grown from methanol solutions. Fig. 10 shows the molecular structures with an atom numbering scheme. In each structure, there is a crystallographic inversion center at the midpoint of N3 and $N3^i$. The molecules are the *E–E* isomers. The nitrogen–nitrogen bonds, N3–$N3^i$ of $H_2L^{2\text{-Me}}$ (1.409(3) Å) and N3–N3* of $H_2L^{2\text{-Et-5-Me}}$ (1.4057(18) Å), can be formally defined as a single bond and compared with the N–N bond distance in hydrazine (1.45 Å). The C–N bonds, C5–N3 of $H_2L^{2\text{-Me}}$ (1.278(4) Å) and C7–N3 of $H_2L^{2\text{-Et-5-Me}}$ (1.284(2) Å), are considered to have full double-bond character. Obviously, in $H_2L^{2\text{-Et-5-Me}}$, upon coordination, the proton is transferred from N2 to N1. In $H_2L^{2\text{-Me}}$, N1 is protonated in contrast to $H_2L^{2\text{-Et-5-Me}}$.

4.2. Structures of the mononuclear complexes

Magnetic studies revealed that the **1H·ClO$_4$** complex remains in the LS state over the whole temperature range, and the molecular structure was determined at 103 K (Fig. 11). The Fe^{II} ion binds two H_2L^H ligands and has a pseudo-octahedral coordination geometry. Each ligand in the *Z–E* configuration serves as a tridentate ligand and coordinates meridionally to the metal ion with two imidazole nitrogen atoms and one azine nitrogen atom, and the other azine nitrogen atom remains uncoordinated (see Scheme 2) [23]. Thus, the H_2L^H ligand becomes unsymmetrical upon coordination to form a five-membered and a six-membered chelate. This creates disor-

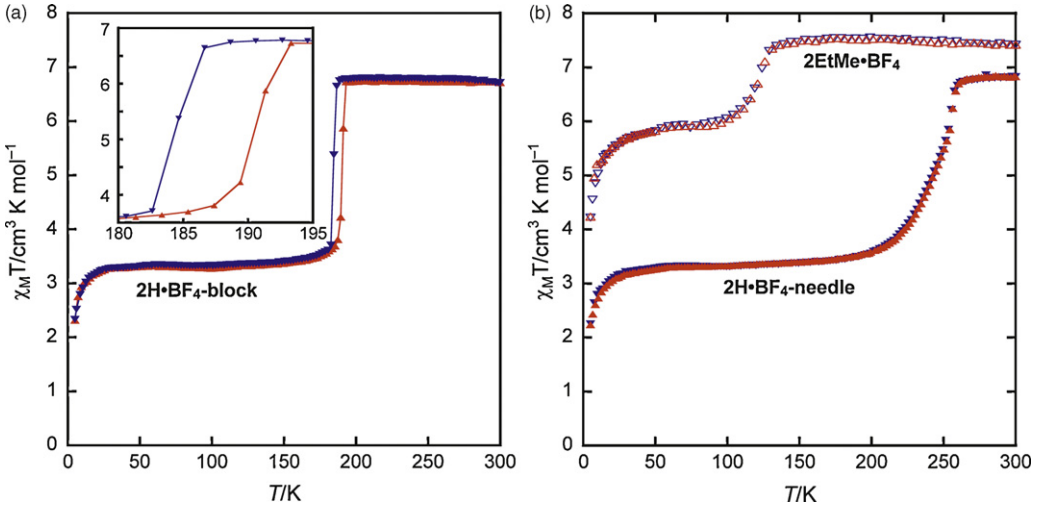

Fig. 8. Magnetic behaviors of (a) block crystals of $[Fe_2(H_2L^H)_3](BF_4)_4$ (**2H·BF$_4$-block**) and (b) needle crystals of $[Fe_2(H_2L^H)_3](BF_4)_4$ (**2H·BF$_4$-needle**) in the form of $\chi_M T$ versus T plots. A hysteresis (inset) is observed in **2H·BF$_4$-block**; $T_c\uparrow = 190$ K and $T_c\downarrow = 183$ K with $\Delta T = 7$ K.

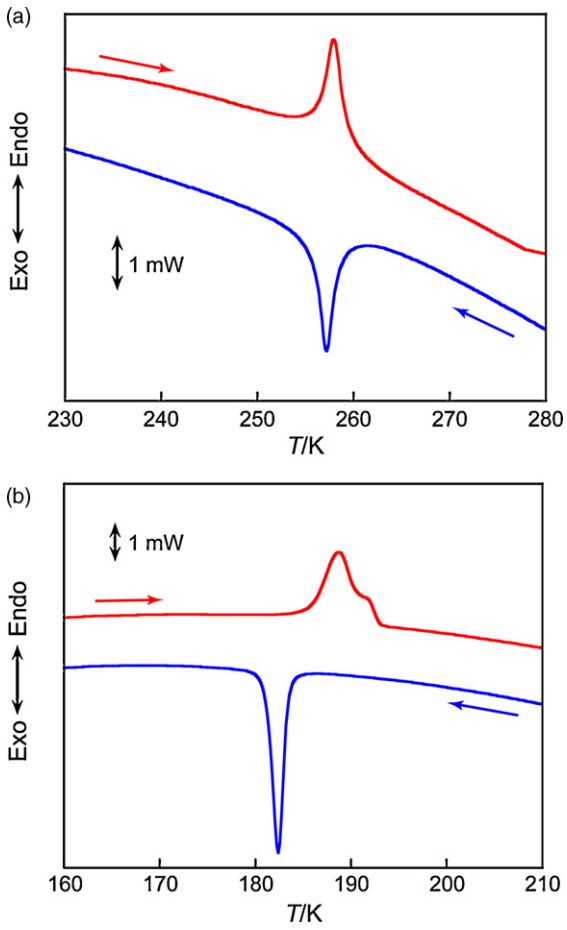

Fig. 9. Differential scanning calorimetry curves in the spin crossover region for (a) the needle crystals and (b) the block crystals of $[Fe_2(H_2L^H)_3](BF_4)_4$ (**2H·BF$_4$**); the red and blue curves correspond to the DCS data in the heating and cooling modes, respectively. Reproduced with permission from Ref. [17b].

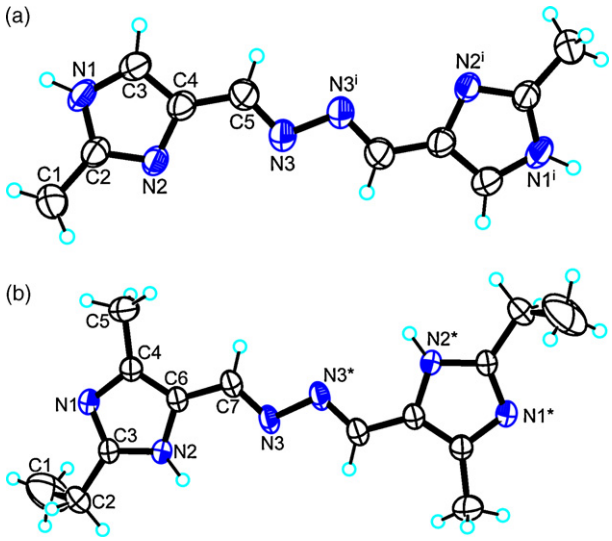

Fig. 10. X-ray molecular structures of (a) $H_2L^{2\text{-Me}}$ and (b) $H_2L^{2\text{-Et-5-Me}}$ with atom numbering scheme.

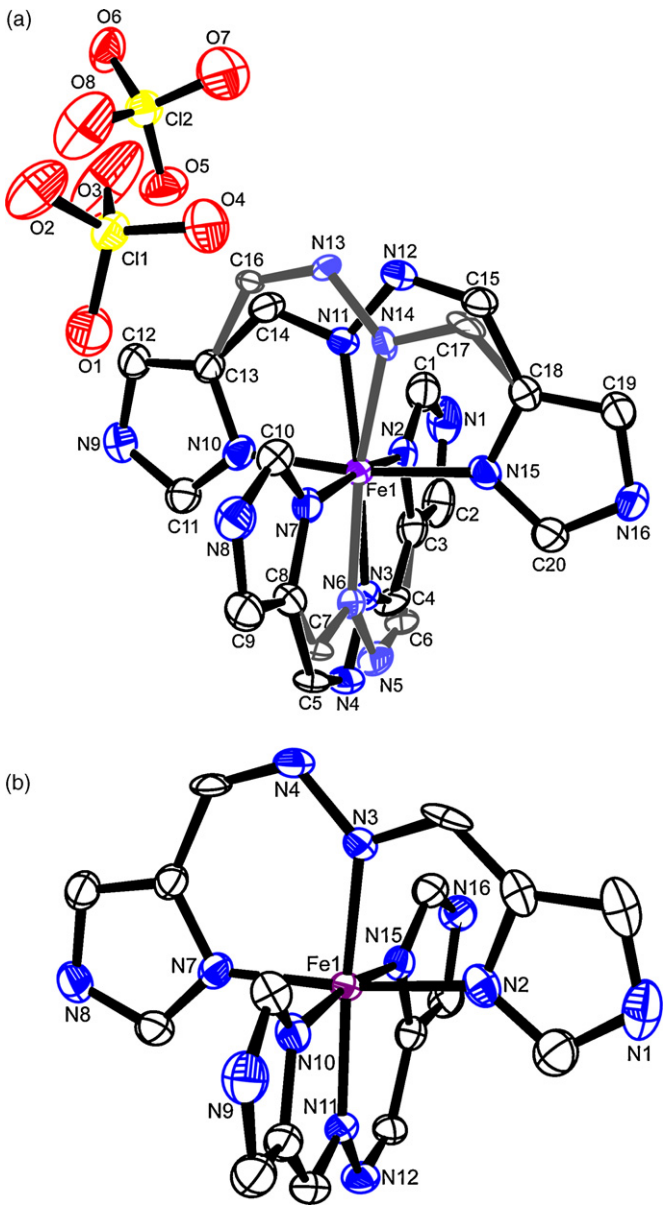

Fig. 11. (a) X-ray molecular structure of $[Fe(H_2L^H)_2](ClO_4)_2{\cdot}2CH_3CN$ (**1H·ClO$_4$**) with an atom numbering scheme showing the 50% probability ellipsoids. The hydrogen atoms and acetonitrile molecules have been omitted for clarity. Color code—purple: LS Fe; blue: N; black: C, yellow: Cl; and red: O. The structure suffers from disorder at the azine moieties. (b) X-ray molecular structure of the cation of **1H·ClO$_4$** with larger Occ values.

der in the moieties involving azine: C4–N3–N4–C5 (Occ = 0.56) and C6–N5–N6–C7 (Occ = 0.44), and C14–N11–N12–C15 (Occ = 0.78) and C16–N13–N14–C17 (Occ = 0.22). All of the Fe–N coordinate bond distances (1.950(2)–2.021(12) Å) are typical for LS Fe^{II} [24] in accordance with the magnetic study. Fig. 11(b) shows the cation of **1H·ClO$_4$** with larger Occ values.

Fig. 12 compares intramolecular steric interactions in **1H·ClO$_4$**, **1Me·ClO$_4$**, and **1EtMe·ClO$_4$**. The X-ray crystal structure analyses of **1Me·ClO$_4$** and **1EtMe·ClO$_4$** were carried out at 200 K and 193 K, respectively, because magnetic studies revealed that they stay in the HS state in the 5–300 K temperature range. In Fig. 12, one of the ligands of each complex cation is in the plane of the paper, and the other ligand is perpendicular to the paper. The N2–Fe1–N7 bond of **1H·ClO$_4$** is almost linear (172.73(9)°), while the corresponding bond of **1Me·ClO$_4$** is bent (161.29(11)°), and the latter is attributable to the steric effect of the methyl group. The least-squares plane

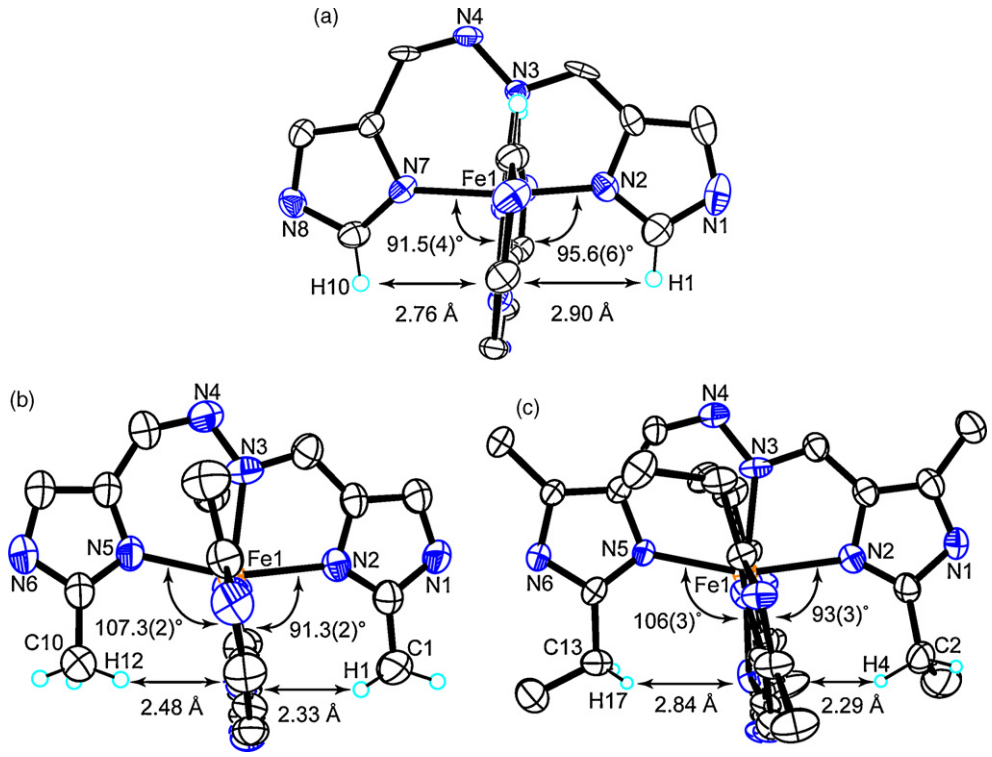

Fig. 12. Comparison of the intramolecular steric interactions in (a) $[Fe(H_2L^H)_2](ClO_4)_2{\cdot}2CH_3CN$ (**1H·ClO$_4$**), (b) $[Fe(H_2L^{2\text{-Me}})_2](ClO_4)_2{\cdot}1.6CH_3CN$ (**1Me·ClO$_4$**), and (c) $[Fe(H_2L^{2\text{-Et-5-Me}})_2](ClO_4)_2{\cdot}CH_3OH$ (**1EtMe·ClO$_4$**). Severe steric repulsion exists between a methyl group of an $H_2L^{2\text{-Me}}$ ligand and the other $H_2L^{2\text{-Me}}$ ligand in **1Me·ClO$_4$**, and between an ethyl group of an $H_2L^{2\text{-Et-5-Me}}$ ligand and the other $H_2L^{2\text{-Et-5-Me}}$ ligand in **1EtMe·ClO$_4$**.

(P_L) of the $H_2L^{2\text{-Me}}$ ligand (or the H_2L^H ligand), which is perpendicular to the paper, and the angles between P_L and Fe–N2 and Fe–N7 or Fe–N5 were defined as in Fig. 12. The angle between P_L and Fe–N5 for **1Me·ClO$_4$** (107.3(2)°) is much larger than the corresponding angle between P_L and Fe–N7 for **1H·ClO$_4$** (91.5(4)°) because of steric effects. To cope with the steric crowding, the $H_2L^{2\text{-Me}}$ ligand deviates from planarity, as evidenced by Fig. 12(b). Such steric crowding will lengthen the Fe–N bond, resulting in the HS state. Thus, the unusual order in ligand field strength, $H_2L^H > H_2L^{2\text{-Me}}$, in the mononuclear complexes can be accounted for by steric effects causing lengthening of the Fe–N bond. The situation of **1EtMe·ClO$_4$** is very similar to that of **1Me·ClO$_4$**, and thus both complexes are in the HS state in the temperature range 30–300 K. The spin states of these complexes remain unchanged in solution, as evidenced by the UV–vis spectra.

4.3. Structures of the dinuclear complexes

Because **2H·ClO$_4$** shows SCO around 240 K, the X-ray crystal structure analysis was carried out at two temperatures, 103 K and 293 K. The same space group, $P2_1/c$ (no. 14), is retained at both temperatures. Selected bond lengths and angles are collated in Table 2. Fig. 13 shows an ORTEP drawing of the cation of **2H·ClO$_4$** at 293 K, with the atom numbering scheme. The cation shows a dinuclear triple-helicate structure, with each ligand bound as a bis(bidentate) ligand to two different iron centers. Each Fe^{II} center binds to three ligand strands to attain a pseudo-octahedral coordination geometry. Each complex is chiral, with either a Δ (clockwise) or a Λ (anticlockwise) configuration because of the screw coordination arrangement of the three ligands around Fe^{II}. Both iron centers shown in Fig. 13 have the Λ configuration, and thus this is a homochiral Λ–Λ pair. Because the complex crystallizes in a centrosymmetric space group, $P2_1/c$, molecules with the Δ–Δ and Λ–Λ pairs coexist in the crystal to form a racemic crystal. In other words, **2H·ClO$_4$** does not undergo spontaneous resolution. All of the Fe–N coordinate bond distances (2.116(2)–2.238(2) Å) are in the range for HS Fe^{II} [24]. The two iron centers, Fe1 and Fe2, are in different environments. The average Fe1–N bond length (2.153 Å) is shorter than that of Fe2–N (2.197 Å) at 293 K.

Table 2
Relevant bond lengths (Å) and angles (deg) with their estimated standard deviations in parentheses for $[Fe_2(H_2L^H)_3](ClO_4)_4{\cdot}5CH_3NO_2$ (**2H·ClO$_4$**) at 103 and 293 K.

Bond lengths (Å)					
	Fe–N(imidazole)			Fe–N(azine)	
	293 K	103 K		293 K	103 K
Fe(1)–N(2)	2.116(2)	1.979(3)	Fe1–N3	2.187(2)	1.971(3)
Fe(1)–N(8)	2.116(2)	1.972(3)	Fe(1)–N(9)	2.177(2)	1.972(2)
Fe(1)–N(14)	2.122(2)	1.979(2)	Fe(1)–N(15)	2.196(2)	1.977(3)
Fe(2)–N(4)	2.238(2)	2.215(3)	Fe(2)–N(5)	2.142(2)	2.150(3)
Fe(2)–N(10)	2.238(2)	2.221(3)	Fe(2)–N(11)	2.151(2)	2.157(2)
Fe(2)–N(16)	2.238(2)	2.218(3)	Fe(2)–N(17)	2.175(2)	2.174(3)
Fe(1)···Fe(2)	4.0362(7)	3.8507(8)			

Bond angles (deg)		
	293 K	103 K
N(2)–Fe(1)–N(3)	75.26(10)	80.03(13)
N(8)–Fe(1)–N(9)	75.65(10)	80.27(12)
N(14)–Fe(1)–N(15)	75.18(10)	80.07(12)
N(4)–Fe(2)–N(5)	74.33(10)	74.15(12)
N(10)–Fe(2)–N(11)	73.79(9)	73.89(11)
N(16)–Fe(2)–N(17)	74.00(9)	74.35(11)

Torsion angles (deg)		
	293 K	103 K
C(4)–N(3)–N(4)–C(5)	63.6(3)	62.2(4)
C(12)–N(9)–N(10)–C(13)	62.7(3)	58.8(4)
C(20)–N(15)–N(16)–C(21)	51.8(3)	48.4(4)

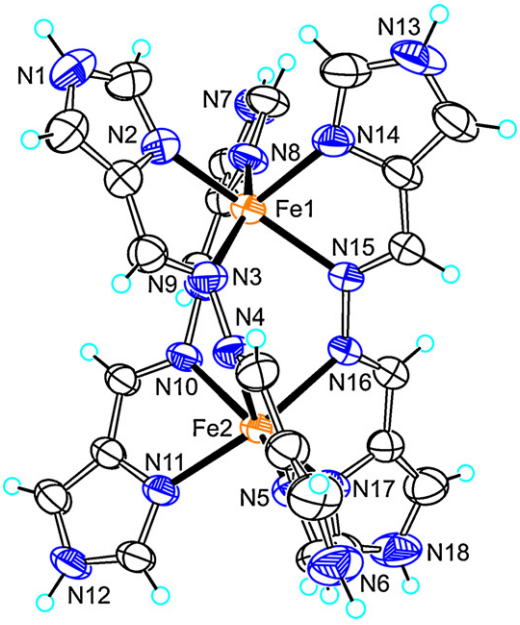

Fig. 13. X-ray molecular structure of the cation of $[Fe_2(H_2L^H)_3](ClO_4)_4{\cdot}5CH_3NO_2$ (**2H·ClO$_4$**) at 293 K with an atom numbering scheme showing the 50% probability ellipsoids. Color code—orange: HS Fe, blue: N, black: C, and light blue: H.

At 103 K, the average Fe1–N bond length (1.975 Å) is shorter by 0.178 Å than that at 293 K (2.153 Å), demonstrating that the SCO occurs at the Fe1 site, while the Fe2 site remains in the HS state (average Fe2–N bond length = 2.189 Å), to form a mixed-spin state [LS–HS] complex. The N–Fe1–N five-membered chelate angles (average angle = 80.12°) are larger than the N–Fe2–N angles (average angle = 74.13°), and the octahedron is markedly less distorted at the LS Fe1 site than at the HS Fe2 site. The intraligand dihedral angles between the two imidazolylimine groups decrease with decreasing temperature from 50.5(1)°, 53.2(1)°, and 41.5(1)° at 293 K to 47.4(2)°, 47.6(1)°, and 38.1(2)° at 103 K. The Fe1···Fe2 distance decreases from 4.0362(7) Å at 293 K to 3.8507(8) Å at 103 K. The unit cell volume of 5610.1(3) Å^3 at 293 K decreases to 5344.3(5) Å^3 at 103 K (4.7%).

Close inspection of the crystal structure at 103 K (Fig. 14) suggests a factor that stabilizes the [LS–HS] state. The dinuclear complex is linked to neighboring dinuclear units by hydrogen bonds to form a zigzag 1D structure along the *c*-axis. Fe1 and Fe2 are in different environments and the two neighboring Fe1 sites are effectively linked by hydrogen bonds. In a previous paper, we showed that the effect of hydrogen bonds is similar to that of ligand deprotonation: it stabilizes the LS state [8f]. Thus, Fe1 tends to assume the LS state and the mixed-spin [LS–HS] state is stabilized.

The X-ray crystal structure analysis of **2Me·ClO$_4$** at 293 K showed that the Fe–N coordinate bond distances (1.936(2) Å and 1.989(2) Å) are typical for LS Fe^{II}, and the average (1.963 Å) is close to that of the LS site for **2H·ClO$_4$** at 103 K (1.975 Å). These results are in agreement with the magnetic result. The N–Fe1–N five-membered chelate angle (79.94°) is also close to that of the average (80.12°) for the LS site for **2H·ClO$_4$** at 103 K. The Fe(LS)···Fe(LS) distance (3.4842(7) Å) is much smaller than the Fe(LS)···Fe(HS) distance (3.8507(8) Å) for **2H·ClO$_4$** at 103 K. Unlike the mononuclear complex $[Fe(H_2L^{2\text{-}Me})_2](ClO_4)_2{\cdot}1.6CH_3CN$ (**1Me·ClO$_4$**), **2Me·ClO$_4$** involves no significant intramolecular steric repulsion between the methyl groups of an $H_2L^{2\text{-}Me}$ ligand and the other ligands (Fig. 15). The $H_2L^{2\text{-}Me}$ ligand involving an electron-donating methyl group on each imidazole group exerts a greater ligand field strength than the H_2L^H ligand. Thus, **2Me·ClO$_4$** is in the LS state even at room temperature.

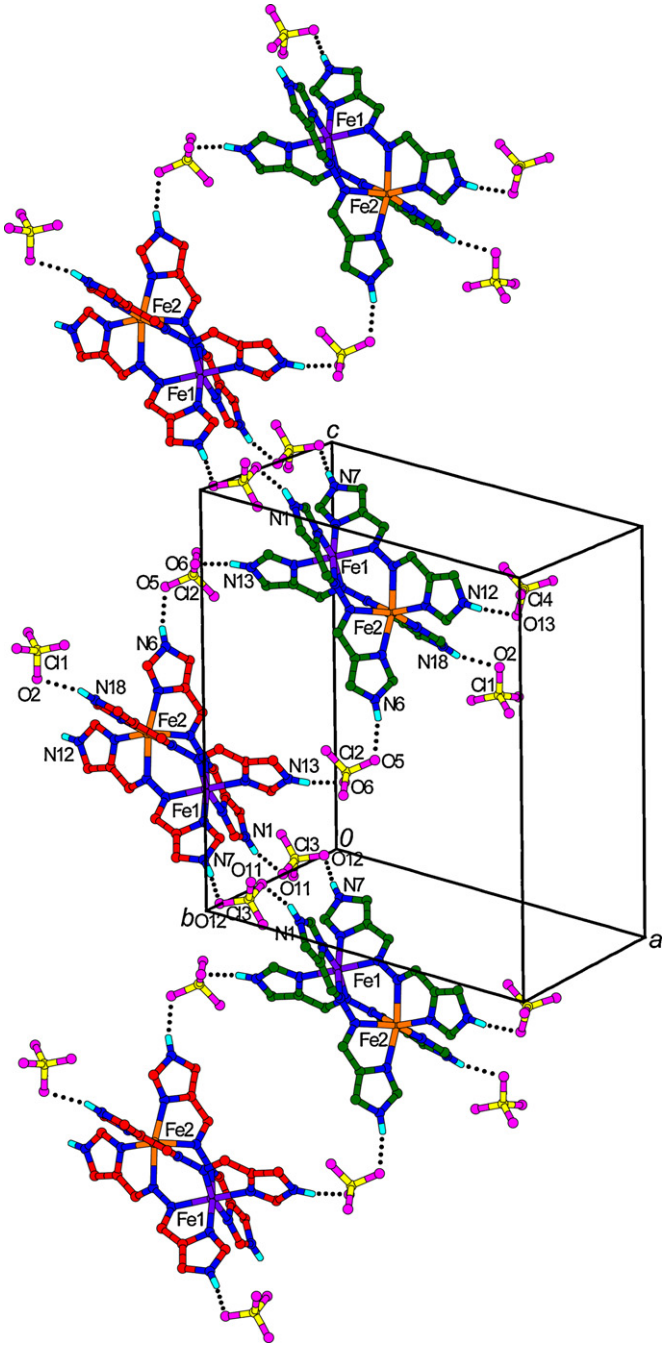

Fig. 14. Crystal structure of $[Fe_2(H_2L^H)_3](ClO_4)_4{\cdot}5CH_3NO_2$ (**2H·ClO$_4$**) at 103 K, with a selected atom numbering scheme. Perchlorate anions and solvent molecules not participating in hydrogen bonding have been omitted for clarity. Color code—orange: HS Fe; purple: LS Fe; blue: N; light blue: H; yellow: Cl; pink: O. The red and green colored molecules denote the Λ–Λ and △–△ pair, respectively. Reproduced with permission from Ref. [17b].

As described above, two types of crystals, plates and blocks, were isolated for **2EtMe·ClO$_4$**, and they were separated manually under a microscope. The X-ray crystal structure analysis of the plate crystals of $[Fe_2(H_2L^{2\text{-}Et\text{-}5\text{-}Me})_3](ClO_4)_4{\cdot}0.5H_2O{\cdot}3CH_3CN$ (**2EtMe·ClO$_4$-plate**) was carried out at 163 K. The overall molecular structure is similar to that of **2H·ClO$_4$** at 103 K. The two Fe^{II} centers, Fe1 and Fe2, are in different environments. The Fe1–N bond lengths (2.154(3)–2.210(3) Å) and Fe2–N bond lengths (1.969(3)–2.036(3) Å) are typical for HS Fe^{II} and LS Fe^{II}, respectively. The complex assumes a mixed-spin [LS–HS] state at 163 K, in contrast to the

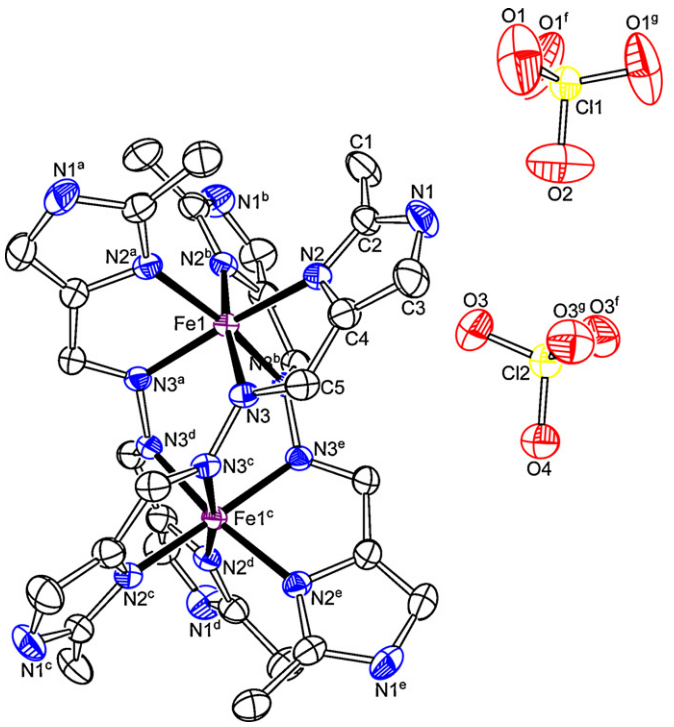

Fig. 15. X-ray molecular structure of the cation of $[Fe_2(H_2L^{2\text{-Me}})_3](ClO_4)_4$ (**2Me·ClO$_4$**) with an atom numbering scheme showing the 50% probability ellipsoids. The hydrogen atoms have been omitted for clarity. Color code—purple: LS Fe; blue: N; black: C, yellow: Cl; and red: O.

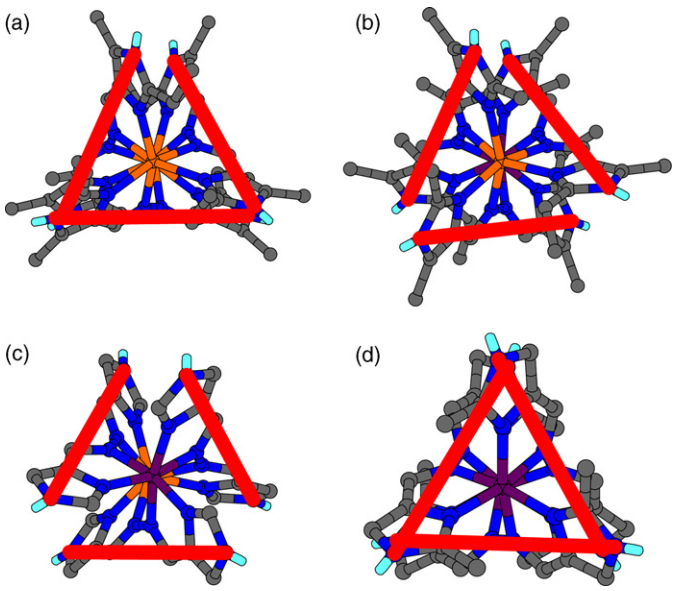

Fig. 16. Comparison of the dinuclear complex cations as projected down the approximate threefold axis. (a) $[Fe_2(H_2L^{2\text{-Et-5-Me}})_3](ClO_4)_4{\cdot}2CH_3CN$ (**2EtMe·ClO$_4$-block**) at 113 K, (b) $[Fe_2(H_2L^{2\text{-Et-5-Me}})_3](ClO_4)_4{\cdot}H_2O{\cdot}3CH_3CN$ (**2EtMe·ClO$_4$-plate**) at 163 K, (c) $[Fe_2(H_2L^{H})_3](BF_4)_4{\cdot}6.5CH_3NO_2{\cdot}0.5H_2O$ (**2H·BF$_4$**) at 173 K, and (d) $[Fe_2(H_2L^{2\text{-Me}})_3](ClO_4)_4$ (**2Me·ClO$_4$**) at 293 K. Color code—purple: LS Fe; orange: HS Fe; blue: N; gray: C. Reproduced with permission from Ref. [18].

magnetic study. The magnetic study revealed that the complex exhibited an abrupt spin transition at ca. 120 K, and thus we expected the [HS–HS] state at 163 K. This discrepancy seems to be related to the efflorescent nature of the crystals. The acetonitrile molecules involved in the crystals are easily lost on standing in air, and the sample thus obtained, ($[Fe_2(H_2L^{2\text{-Et-5-Me}})_3](ClO_4)_4{\cdot}H_2O$), was used for the magnetic measurements. It has been pointed out that solvent molecules play an important role in the SCO behavior [5e,11].

The X-ray crystal structure analysis of the block crystals of $[Fe_2(H_2L^{2\text{-Et-5-Me}})_3](ClO_4)_4{\cdot}2CH_3CN$ (**2EtMe·ClO$_4$-block**) was carried out at 113 K. The Fe–N bond lengths are in the range of 2.126(2)–2.302(2) Å, demonstrating that the complex is in the [HS–HS] state. The molecular structure is similar to that of **2H·ClO$_4$** at 293 K. The crystal-packing diagram shows that hydrogen bonds and CH–π interactions form a 3D structure. Because of these intermolecular interactions, the complex is severely distorted (see below).

When $[Fe_2(H_2L^{H})_3](BF_4)_4$ (**2H·BF$_4$**) was crystallized from nitromethane by slow diffusion of diethyl ether, two kinds of crystals (polymorphs), needles and blocks, were obtained. We determined the structure of the block crystals (**2H·BF$_4$-block**) by X-ray diffraction. The block crystals exhibited an abrupt spin transition at about 190 K, and we determined the structure at 173 K. The complex assumes a mixed-spin [LS–HS] state at 173 K, and thus the molecular structure is similar to that of **2H·ClO$_4$** at 103 K, which also has a mixed-spin [LS–HS] state. The Fe1–N bond lengths (1.965(2)–1.987(3) Å) and Fe2–N bond lengths (2.144(3)–2.247(6) Å) are typical for LS Fe^{II} and HS Fe^{II}, respectively.

The crystal-packing diagram of **2H·BF$_4$-block** shows that all six imidazole N–H groups of a $[Fe_2(H_2L^{H})_3]^{4+}$ complex cation are connected to the BF_4^- anions by hydrogen bonds to form a homochiral 2D sheet structure. It is well established that the elastic interaction between SCO sites within a crystal lattice is the predominant factor governing cooperativity. The abrupt spin transition accompanied by hysteresis (Fig. 8) observed for the block crystals may be accounted for by the 2D sheet structure involving strong intermolecular interactions.

Fig. 16 compares the distortion of the dinuclear complex cations, **2EtMe·ClO$_4$-block**, **2EtMe·ClO$_4$-plate**, **2H·BF$_4$-block**, and **2Me·ClO$_4$**, as projected down the approximate threefold axis. Uncoordinated imidazole nitrogen atoms of each ligand are connected by red lines. Fig. 16 clearly shows that the dinuclear complexes with $H_2L^{2\text{-Et-5-Me}}$ (**2EtMe·ClO$_4$-block**, **2EtMe·ClO$_4$-plate**) have less symmetrical structures about the pseudo-C_3 axis of the molecule than those of the related complexes of **2H·BF$_4$** and **2Me·ClO$_4$**. The average torsion angles around the azine N–N bonds for dinuclear complexes **2EtMe·ClO$_4$** ([LS–HS] state: 60(2)° for **2EtMe·ClO$_4$-plate**; [HS–HS] state: 77(6)° for **2EtMe·ClO$_4$-block**) are larger than those of **2H·X** ([LS–HS] state: 56(1)° for **2H·BF$_4$**, 57(4)° for **2H·ClO$_4$** at 103 K; [HS–HS] state: 59(4)° for **2H·ClO$_4$** at 293 K). As a result of these distortions, the average Fe–N bond lengths of **2EtMe·ClO$_4$** (2.20 Å for the HS site; 2.01 Å for the LS site) are slightly larger than those of **2H·X** (2.18 Å for the HS site; 1.98 Å for the LS site). This fact indicates that the electronic effect of the substituent is outweighed by the steric effect and the ligand field strength of $H_2L^{2\text{-Et-5-Me}}$ is weakened. In the two **2EtMe·ClO$_4$** complexes, **2EtMe·ClO$_4$-block** is more distorted from C_3 symmetry, probably because of the hydrogen bonds and CH–π interactions in the crystal structure. Such a distortion lengthens the Fe–N bond, resulting in the HS state being favored.

5. Conclusion

Imidazole-4-carbaldehyde azine and its derivatives, H_2L^R (R = H, 2-Me, 5-Me, 2-Et-5-Me), were prepared by condensation of 4-formylimidazole, or its derivatives, 2-methyl- or 5-methyl-4-formylimidazole, or 2-ethyl-4-methyl-5-formylimidazole, with hydrazine in a 2:1 mole ratio in methanol. The H_2L^R ligands are imidazole analogues of PAA. The H_2L^R ligands afforded mononuclear $[Fe(H_2L^R)_2]^{2+}$ and dinuclear triple-helicate $[Fe_2(H_2L^R)_3]^{4+}$ complexes, and their magnetostructural relationships were studied. In

contrast to $[Fe(PAA)_2]^{2+}$ and $[Fe_2(PAA)_3]^{4+}$, both of which are in the LS state, the H_2L^R complexes showed a variety of magnetic behaviors depending on such factors as the nuclearity, the kind of substituents, counterions, and crystal solvents. When a hydrogen atom at the 2-position of imidazole in H_2L^H is replaced by an electron-donating methyl group, the ligand field strength becomes stronger and the complex tends to assume the LS state. This trend was observed in the dinuclear complexes; $[Fe_2(H_2L^H)_3]^{4+}$ and $[Fe_2(H_2L^{2\text{-}Me})_3]^{4+}$ assume the [HS–HS] and [LS–LS] spin states, respectively, at room temperature. However, the mononuclear Fe^{II} complexes, $[Fe(H_2L^H)_2]^{2+}$ and $[Fe(H_2L^{2\text{-}Me})_2]^{2+}$, afforded a different order of ligand field strengths; $[Fe(H_2L^H)_2]^{2+}$ is in the LS state while $[Fe(H_2L^{2\text{-}Me})_2]^{2+}$ is in the HS state at room temperature. X-ray structural studies revealed that the interligand steric repulsion between a methyl group of an $H_2L^{2\text{-}Me}$ ligand and the other ligand in $[Fe(H_2L^{2\text{-}Me})_2]^{2+}$ is responsible for the observed change in the spin state. In this case, the steric effect outweighs the electron-donating effect of the methyl group. $[Fe_2(H_2L^H)_3]X_4$ ($X = ClO_4$, BF_4) exhibited a sharp spin transition, [LS–HS] ↔ [HS–HS], and the existence of the mixed-spin state [LS–HS] was confirmed from X-ray crystallographic data. In summary, the present study showed that the steric effect plays an important role in determining the spin state of the complex: steric crowding lengthens the Fe–N bond to decrease the ligand field strength, resulting in the HS state being favored.

Acknowledgments

This work was supported by a Grant-in-Aid for Scientific Research (Nos. 16205010, 17350028 and 20550064) from the Ministry of Education, Science, Sports, and Culture of Japan.

References

[1] (a) O. Kahn, C.J. Martinez, Science 279 (1998) 44;
(b) S. Hayami, K. Danjobara, K. Inoue, Y. Ogawa, N. Matsumoto, Y. Maeda, Adv. Mater. 16 (2004) 869;
(c) J.F. Létard, P. Guionneau, L. Goux-Capes, in: P. Gütlich, H.A. Goodwin (Eds.), Topics in Current Chemistry, 235, Springer-Verlag, Berlin, 2004, p. 221;
(d) V. Niel, J.M. Martinez-Agudo, M.C. Muñoz, A.B. Gaspar, J.A. Real, Inorg. Chem. 40 (2001) 3838.
[2] L. Cambi, L. Szegö, Ber 66 (1933) 657.
[3] (a) P.E. Figgins, D.H. Busch, J. Am. Chem. Soc. 82 (1960) 820;
(b) M.A. Robinson, J.D. Curry, D.H. Busch, Inorg. Chem. 2 (1963) 1178.
[4] R.C. Stoufer, D.H. Busch, W.B. Hadley, J. Am. Chem. Soc. 83 (1961) 3732.
[5] (a) E. König, Prog. Inorg. Chem. 35 (1987) 527;
(b) E. König, Struct. Bonding (Berlin) 76 (1991) 51;
(c) H.A. Goodwin, Coord. Chem. Rev. 18 (1976) 293;
(d) P. Gütlich, A. Hauser, H. Spiering, Angew. Chem., Int. Ed. Engl. 33 (1994) 2024;
(e) J.A. Real, A.B. Gaspar, V. Niel, M.C. Muñoz, Coord. Chem. Rev. 236 (2003) 121;
(f) G. Lemercier, M. Verelst, A. Bousseksou, F. Varret, J.-P. Tuchagues, in: O. Kahn (Ed.), "Magnetism: A Supramolecular Function", NATO ASI Series, Series C 484, Kluwer Academic Publ., Dordrecht (Pays-Bas), 1996, p. 335;
(g) P. Gütlich, Y. Garcia, T. Woike, Coord. Chem. Rev. 219–221 (2001) 839;
(h) P. Gütlich, H.A. Goodwin (Eds.), Topics in Current Chemistry, 233–235, Springer-Verlag, Berlin, 2004;
(i) J.A. Real, A.B. Gaspar, M.C. Muñoz, Dalton Trans. (2005) 2062;
(j) G. Vanko, F. Renz, G. Molnar, T. Neisius, S. Karpati, Angew. Chem., Int. Ed. 46 (2007) 5306;
(k) A. Bousseksou, N. Negre, M. Goiran, L. Salmon, J.-P. Tuchagues, M.-L. Boillot, K. Boukheddaden, F. Varret, Eur. Phys. J. B13 (2000) 451;
(l) P. Gamez, J.S. Costa, M. Quesada, G. Aromí, Dalton (2009) 7845;
(m) S. Brooker, J.A. Kitchen, Dalton (2009) 7331;
(n) K.S. Murray, Aust. J. Chem. 62 (2009) 1081;
(o) A.B. Gaspar, Coord. Chem. Rev. 253 (2009) 2399;
(p) M. Ohba, K. Yoneda, G. Agustí, M.C. Muñoz, A.B. Gaspar, J.A. Real, M. Yamasaki, H. Ando, Y. Nakao, S. Sakaki, S. Kitagawa, Angew. Chem., Int. Ed. 48 (2009) 4767;
(q) P.D. Southon, L. Liu, E.A. Fellows, D.J. Price, G.J. Halder, K.W. Chapman, B. Moubaraki, K.S. Murray, J.-F. Ltard, C.J. Kepert, J. Am. Chem. Soc. 131 (2009) 10998.
[6] (a) W.J. Stratton, D.H. Busch, J. Am. Chem. Soc. 80 (1958) 1286;
(b) W.J. Stratton, D.H. Busch, J. Am. Chem. Soc. 80 (1958) 3191;
(c) W.J. Stratton, D.H. Busch, J. Am. Chem. Soc. 82 (1960) 4834.
[7] J. Hamblin, A. Jackson, N.W. Alcock, M.J. Hannon, J. Chem. Soc., Dalton Trans. (2002) 1635.
[8] (a) Y. Sunatsuki, M. Sakata, S. Matsuzaki, N. Matsumoto, M. Kojima, Chem. Lett. (2001) 1254;
(b) Y. Sunatsuki, Y. Ikuta, N. Matsumoto, H. Ohta, M. Kojima, S. Iijima, S. Hayami, Y. Maeda, S. Kaizaki, F. Dahan, J.-P. Tuchagues, Angew. Chem., Int. Ed. 42 (2003) 1614;
(c) H. Ohta, Y. Sunatsuki, Y. Ikuta, N. Matsumoto, S. Iijima, H. Akashi, T. Kambe, M. Kojima, Mater. Sci. 21 (2003) 191;
(d) Y. Ikuta, M. Ooidemizu, Y. Yamahata, M. Yamada, S. Osa, N. Matsumoto, S. Iijima, Y. Sunatsuki, M. Kojima, F. Dahan, J.-P. Tuchagues, Inorg. Chem. 42 (2003) 7001;
(e) M. Yamada, M. Ooidemizu, Y. Ikuta, S. Osa, N. Matsumoto, S. Iijima, M. Kojima, F. Dahan, J.-P. Tuchagues, Inorg. Chem. 42 (2003) 8406;
(f) Y. Sunatsuki, H. Ohta, M. Kojima, Y. Ikuta, Y. Goto, N. Matsumoto, S. Iijima, H. Akashi, S. Kaizaki, F. Dahan, J.-P. Tuchagues, Inorg. Chem. 43 (2004) 4154;
(g) H. Ohta, Y. Sunatsuki, M. Kojima, S. Iijima, H. Akashi, N. Matsumoto, Chem. Lett. 33 (2004) 350;
(h) M. Yamada, E. Fukumoto, M. Ooidemizu, N. Bréfuel, N. Matsumoto, S. Iijima, M. Kojima, N. Re, F. Dahan, J.-P. Tuchagues, Inorg. Chem. 44 (2005) 6967;
(i) M. Yamada, H. Hagiwara, H. Torigoe, N. Matsumoto, M. Kojima, F. Dahan, J.-P. Tuchagues, N. Re, S. Iijima, Chem. Eur. J. 12 (2006) 4536;
(j) S. Iijima, F. Mizutani, O. Niwa, N. Matsumoto, Y. Sunatsuki, M. Kojima, Hyperfine Int. 166 (2007) 397.
[9] A.B. Gaspar, M.C. Muñoz, J.A. Real, J. Mater. Chem. 16 (2006) 2522.
[10] (a) V. Ksenofontov, A.B. Gaspar, V. Niel, S. Reiman, J.A. Real, P. Gütlich, Chem. Eur. J. 10 (2004) 1291;
(b) N. Ortega-Villar, A.L. Thompson, M.C. Muñoz, V.M. Ugalde-Saldivar, A.E. Goeta, R. Moreno-Esparza, J.A. Real, Chem. Eur. J. 11 (2005) 5721;
(c) R. Kitashima, S. Imatomi, M. Yamada, N. Matsumoto, Y. Maeda, Chem. Lett. 34 (2005) 1388;
(d) J.A. Real, H. Bolvin, A. Bousseksou, A. Dworkin, O. Kahn, F. Varret, J. Zarembowitch, J. Am. Chem. Soc. 114 (1992) 4650;
(e) V. Ksenofontov, H. Spiering, S. Reiman, Y. Garcia, A.B. Gaspar, N. Moliner, J.A. Real, P. Gütlich, Chem. Phys. Lett. 348 (2001) 381;
(f) K.S. Murray, Eur. J. Inorg. Chem. (2008) 3101;
(g) J.J. Amoore, C.J. Kepert, J.D. Cashion, B. Moubaraki, S.M. Neville, K.S. Murray, Chem. Eur. J. 12 (2006) 8220;
(h) M.R. Ruben, U. Ziener, J.-M. Lehn, V. Ksenofontov, P. Gütlich, G.B.M. Vaughan, Chem. Eur. J. 11 (2005) 94;
(i) M. Ruben, J. Rojo, F.J. Romero-Salguero, L.H. Uppadine, J.-M. Lehn, Angew. Chem., Int. Ed. 43 (2004) 3644.
[11] K. Nakano, S. Kawata, K. Yoneda, A. Fuyuhiro, T. Yagi, S. Nasu, S. Morimoto, S. Kaizaki, Chem. Commun. (2004) 2892.
[12] M. Klingele, B. Moubaraki, J.D. Cashion, K.S. Murray, S. Brooker, Chem. Commun. (2005) 987.
[13] (a) S.G. Telfer, B. Bocquet, A.F. Williams, Inorg. Chem. 40 (2001) 4818;
(b) L.J. Charbonniere, A.F. Williams, C. Piguet, G. Bernardinelli, E. Rivara-Minten, Chem. Eur. J. 4 (1998) 485.
[14] F. Tuna, M.R. Lees, G.J. Clarkson, M.J. Hannon, Chem. Eur. J. 10 (2004) 5737.
[15] Y. Garcia, C.M. Grunert, S. Reiman, O. van Campenhoudt, P. Gütlich, Eur. J. Inorg. Chem. (2006) 3333.
[16] D. Pelleteret, R. Clérac, C. Mathonière, E. Harté, W. Schmitt, P.E. Kruger, Chem. Commun. (2009) 221.
[17] (a) K. Fujita, R. Kawamoto, R. Tsubouchi, Y. Sunatsuki, M. Kojima, S. Iijima, N. Matsumoto, Chem. Lett. 36 (2007) 1284;
(b) Y. Sunatsuki, R. Kawamoto, K. Fujita, H. Maruyama, T. Suzuki, H. Ishida, M. Kojima, S. Iijima, N. Matsumoto, Inorg. Chem. 48 (2009) 8784.
[18] Y. Sunatsuki, H. Maruyama, K. Fujita, T. Suzuki, M. Kojima, N. Matsumoto, Bull. Chem. Soc. Jpn. 82 (2009) 1497.
[19] K. Nakamoto, Infrared and Raman Spectra of Inorganic and Coordination Compounds, Part B, fifth ed., John Wiley and Sons, New York, 1997.
[20] N.M. Levy, M.C. Laranjeira, A. Neves, C.V. Franco, J. Coord. Chem. 38 (1996) 259.
[21] (a) G.S. Patterson, R.H. Holm, Inorg. Chem. 11 (1972) 2285;
(b) R.F. Handy, R.L. Lintvedt, Inorg. Chem. 13 (1974) 893;
(c) G. Ma, M. Kojima, J. Fujita, Bull. Chem. Soc. Jpn. 62 (1989) 2547.
[22] M.A. Hoselton, L.J. Wilson, R.S. Drago, J. Am. Chem. Soc. 97 (1975) 1722.
[23] R. Karmakar, C.R. Choudhury, S.R. Batten, S. Mitra, J. Mol. Struct. 826 (2007) 75.
[24] J.K. Beattie, Adv. Inorg. Chem. 32 (1988) 1.